A gravity current model with capillary trapping for oil migration in multilayer geological basins

Clément Cancès, David Maltese

A GRAVITY CURRENT MODEL WITH CAPILLARY TRAPPING FOR OIL MIGRATION IN MULTILAYER GEOLOGICAL BASINS

CLÉMENT CANCÈS AND DAVID MALTESE

Abstract. We propose a reduced model accounting capillary trapping to simulate oil migration in geological basins made of several rock types. Our model is derived from Darcy type models thanks to Dupuit approximation and a vertical integration in each geological layer. We propose a time-implicit finite volume scheme which is shown to be unconditionally stable and to admit discrete solutions. Numerical outcomes are then provided in order to illustrate the behavior of our reduced model.

Keywords. Large scale basin modeling, multilayer Dupuit approximation, capillary trapping, Finite Volumes

AMS subjects classification. 65M12, 65M08, 76S05

1. Introduction

1.1. General motivations.

In oil engineering, basin modelling aims at predicting the potential of a geologic area in terms of oil production. The goal is indeed to localize and quantify the presence of hydrocarbons in the porous space of the subsoil. This knowledge can then be used to decide of the exploitation of reservoirs and to optimize the location of the wells. Reconstructing the history of oil migration is therefore an important issue.

In the geological basin context, gravity plays a major role. Hydrocarbons raise within the porous medium to the surface due to buoyancy. Along their migration, they encounter some heterogeneities — typically some changes in the rock properties — that can perturb their progression. For instance, oil can be blocked by impervious (or at least very low permeable) geological structures. But oil can also be trapped in reservoirs because of *capillary barriers*. Capillary barriers correspond to brutal changes of the pore size as illustrated on Figure 1. Such barriers generate forces that are orthogonal to the interface, that can equilibrate with buoyancy. This may yields a quantity of entrapped oil that remains below the capillary barrier.

In the context of basin simulation, dynamics is generally slow. Therefore, Darcean models (see for instance [1]) for immiscible two-phase flows are trustworthy. Such models yields degenerate parabolic problems set on 3-dimensional spatial domains. However, the large time and space scales naturally involved in basin modelling make the resolution of such models very demanding from a computational point of view. This motivates the introduction of reduced models with lower complexity.

A first class of reduced model can be obtained thanks to *ray-tracing*. The ray-tracing method constructs migration flow paths based on the top depth map of a carrier bed (see [25]). The underlying assumption is that hydrocarbon flow-rates and therefore hydrocarbon saturations change very slowly as compared to the duration of simulation time-steps and that migration can therefore be modelled

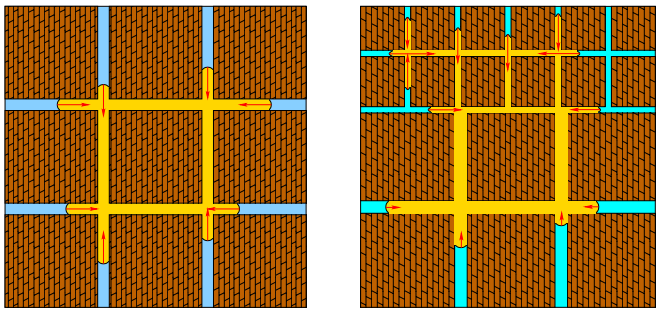

FIGURE 1. Within a homogeneous ideal porous medium with constant pore size, the resulting capillary force on a connected component of non-wetting phase vanishes (left). This is no longer true if the non-wetting phase straddles the interface between two idealized porous media (right): capillarity generates a force orthogonal to the interface.

as a steady state process. A second method is the *invasion percolation* method. Percolation theory can by applied to porous media and deals with the description of interconnections of the porous and fractured network. The percolation invasion introduced in [27] is motivated by the problem of one fluid displacing another from a porous medium under the action of capillary forces. This model has then been extended in [26] by adding the effects of buoyancy. Computationally efficient algorithms have been proposed for instance in [20] for the simulation of invasion percolation.

The history of the migration is kept neither with invasion percolation nor with ray tracing since both reduced models do not keep time as a variable, the goal being to compute directly a steady state, or equivalently a (local) minimizer of the energy since immiscible two-phase flows have a gradient flow structure [6]. The energy, which is made of the gravitational potential energy and the internal energy related to capillarity, is in general non-convex in the McCann's sense [19] when the domain is heterogeneous, so that it may admit several minimizers. It is therefore necessary to compute the whole dynamics to get a trustworthy knowledge of which steady state is relevant. Moreover, reconstructing the history of the migration helps to better predict anomalous pressures in the subsoil. We refer to [23] for an extensive comparison between reduced models and full Darcy models in basin modelling.

In view of the above discussion, our goal is to get a model with reduced complexity while keeping track of the time variable. To this end, we make use of Dupuit approximation, which consists in integrating vertically the equations. This approach is very popular for instance in the community working on carbon dioxyde sequestration [15, 14, 17, 13, 22, 21]. The main unknown is no longer the composition of the fluid, but rather the heights of the free boundaries between the different regions occupied by pure phases. Our models takes into account the variations of the capillary pressure between the different geological layers, allowing capillary trapping. The model is described in next section, whereas its derivation is the purpose of Section 2.

1.2. **Presentation of the reduced model.**

1.2.1. *Geometry of the basin.* In what follows, we assume that the geological basin $\Omega \subset \mathbb{R}^{d+1}$ ($d \in \{1,2\}$) is made of the vertical superposition of I vertical layers $(\Omega_i)_{1\le i\le I}$. We assume that the interface between Ω_i and Ω_{i+1} can be described by $z = b_i(\boldsymbol{x})$, where z denotes the vertical coordinate and $\boldsymbol{x} \in \mathbb{R}^d$ is the horizontal coordinate. We also assume that there exist functions b_0 and b_I corresponding to the lower and upper boundary of Ω_1 and Ω_I respectively. We denote by

$$H_i(\boldsymbol{x}) = b_i(\boldsymbol{x}) - b_{i-1}(\boldsymbol{x})$$

the height of the i^{th} layer Ω_i. To ease the presentation, we assume that

$$\Omega_i = \bigcup_{\boldsymbol{x}\in\mathcal{O}} \{\boldsymbol{x}\} \times (b_{i-1}(\boldsymbol{x}), b_i(\boldsymbol{x})) \tag{1}$$

for some open and bounded set $\mathcal{O} \subset \mathbb{R}^d$.

Two incompressible and immiscible phases (oil and water) flow within each layer Ω_i. Since oil is less dense than water, oil is located on top of the layer, while water occupies its bottom. We assume that the interface separating the oil and the water layers is sharp. The height of the oil layer in Ω_i is then denoted by h_i, and we have naturally that

$$0 \le h_i(t,\boldsymbol{x}) \le H_i(\boldsymbol{x}), \qquad t \ge 0,\ \boldsymbol{x} \in \mathcal{O}.$$

The height of the water layer is then equal to $(H_i - h_i)$. The interface between the two phases is located at

$$z = \gamma_i(t,\boldsymbol{x}) = b_i(\boldsymbol{x}) - h_i(t,\boldsymbol{x}), \qquad t \ge 0,\ \boldsymbol{x} \in \mathcal{O}.$$

We refer to Figure 2 for a schematic depiction of the geometry.

1.2.2. *About the phase pressures.* Water is assumed to be the wetting phase and to be hydrostatic in the whole domain Ω:

$$p_{\mathrm{w}}(t,\boldsymbol{x},z) = -\varrho_{\mathrm{w}} g z, \qquad t \ge 0,\ (\boldsymbol{x},z) \in \Omega, \tag{2}$$

where ϱ_α denotes the density of the phase α and g is the gravity constant. Oil is assumed to be hydrostatic only in the regions where it accumulates, i.e.,

$$p_{\mathrm{o}}(t,\boldsymbol{x},z) = -\varrho_{\mathrm{o}} g z + C_i(t,\boldsymbol{x}), \qquad \gamma_i(t,\boldsymbol{x}) < z < b_i(\boldsymbol{x}).$$

Each porous medium Ω_i is assumed to be poorly graded, so that the capillary pressure can be assumed to be constant equal to π_i as soon as both phases are present and mobile. In particular, denoting by $p_\alpha(t,\boldsymbol{x},z)$ the pressure of phase α at time t and position $(\boldsymbol{x},z) \in \Omega$, this amounts to claim that

$$p_{\mathrm{o}}(t,\boldsymbol{x},\gamma_i(t,\boldsymbol{x})) - p_{\mathrm{w}}(t,\boldsymbol{x},\gamma_i(t,\boldsymbol{x})) = \pi_i \quad \text{if} \quad b_{i-1}(\boldsymbol{x}) < \gamma_i(t,\boldsymbol{x}) < b_i(\boldsymbol{x}). \tag{3}$$

Note that capillary diffusion is neglected in the bulks, making the assumption of sharp interface reasonable.

We infer from the notion of multivalued phase pressure proposed in [8] the conditions

$$p_{\mathrm{o}}(t,\boldsymbol{x},b_i(\boldsymbol{x})) - p_{\mathrm{w}}(t,\boldsymbol{x},b_i(\boldsymbol{x})) \le \pi_i \quad \text{if} \quad h_i(t,\boldsymbol{x}) = 0, \tag{4a}$$

$$p_{\mathrm{o}}(t,\boldsymbol{x},b_{i-1}(\boldsymbol{x})) - p_{\mathrm{w}}(t,\boldsymbol{x},b_{i-1}(\boldsymbol{x})) \ge \pi_i \quad \text{if} \quad h_i(t,\boldsymbol{x}) = H_i(\boldsymbol{x}). \tag{4b}$$

Therefore, combining (3) with (4), we obtain that

$$p_{\mathrm{o}}(t,\boldsymbol{x},\gamma_i(t,\boldsymbol{x})) - p_{\mathrm{w}}(t,\boldsymbol{x},\gamma_i(t,\boldsymbol{x})) \in \widetilde{\pi}_i(\boldsymbol{x},h_i(t,\boldsymbol{x})), \tag{5}$$

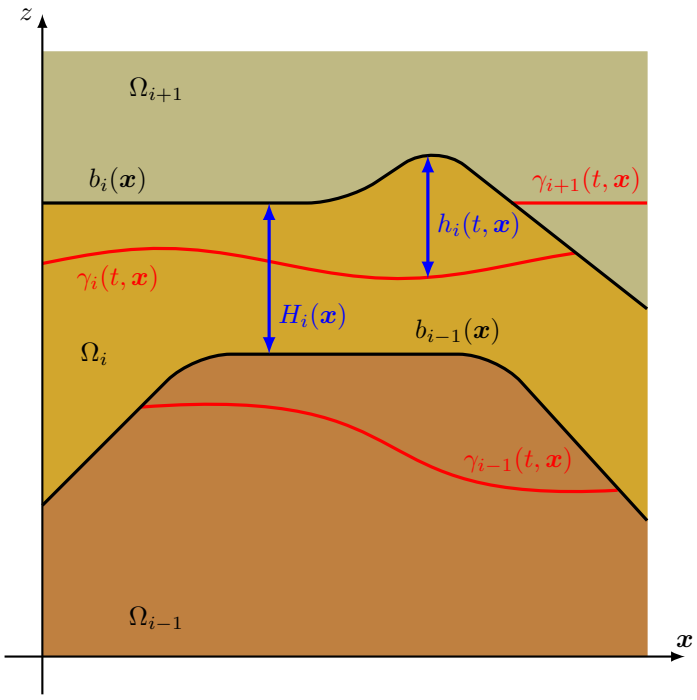

FIGURE 2. Schematic representation of the multilayer geological basin. The interfaces between the i^{th} and the $(i+1)^{\text{th}}$ layer is located at $z = b_i(\boldsymbol{x})$. Inside the layer Ω_i, oil is located above the interface $z = \gamma_i(t,\boldsymbol{x})$, whereas water is located below.

where, for all $\boldsymbol{x} \in \mathcal{O}$, $\widetilde{\pi}_i(\boldsymbol{x},\cdot)$ is the maximal monotone graph defined by

$$\widetilde{\pi}_i(\boldsymbol{x},h) = \begin{cases} \pi_i & \text{if } 0 < h < H_i(\boldsymbol{x}), \\ (-\infty,\pi_i] & \text{if } h = 0, \\ [\pi_i,+\infty) & \text{if } h = H_i(\boldsymbol{x}). \end{cases} \tag{6}$$

Hence, introducing the differential of the densities $\varrho = \varrho_{\mathrm{w}} - \varrho_{\mathrm{o}} > 0$, we get that

$$p_{\mathrm{o}}(t,\boldsymbol{x},z) - p_{\mathrm{w}}(t,\boldsymbol{x},z) = p_i(t,\boldsymbol{x}) + \varrho g(z - \gamma_i(t,\boldsymbol{x})), \qquad \gamma_i(t,\boldsymbol{x}) \le z \le b_i(\boldsymbol{x})$$

with

$$p_i(t,\boldsymbol{x}) \in \widetilde{\pi}_i(\boldsymbol{x}, h_i(t,\boldsymbol{x})), \qquad t \ge 0,\ \boldsymbol{x} \in \mathcal{O}. \tag{7}$$

1.2.3. *Equations governing the motion of the interfaces.* We have at hand the necessary material to state the equation describing the evolution of the interfaces γ_i. The main unknowns are the heights $(h_i)_{1\le i\le I}$ of the oil layers. Denote by ϕ_i and κ_i the porosity and the permeability of the i^{th} layer (which are assumed to be constant), by μ_α the viscosity of the phase α, and by $\varrho = \varrho_w - \varrho_o > 0$ the difference of the densities. Then using Dupuit approximation (cf. Section 2.2), we obtain the following equations for $i \in \{1,\dots,I\}$:

$$\phi_i \partial_t h_i - \nabla\cdot\left(\frac{\kappa_i}{\mu_{\mathrm{o}}} h_i \nabla(p_i + \varrho g(h_i - b_i))\right) = S_{i-1} - S_i, \tag{8}$$

where p_i satisfies (7).

The right-hand-side in (8) represents the interaction between the different layers. More precisely, S_i denotes the oil flux across the interface b_i between Ω_i and Ω_{i+1}. It is computed thanks to formula

$$S_i = \frac{\kappa_i}{\mu_w \frac{\kappa_i}{\kappa_{i+1}} H_{i+1} + \mu_o h_i} \Big(\varrho g h_i - (p_{i+1} - p_i) \Big)^+, \qquad 1 \le i \le I-1, \tag{9}$$

where $a^+ = \max(a, 0)$ denotes the positive part of $a \in \mathbb{R}$.

Remark 1.1. *Formula (9), whose derivation is the purpose of Section 2.3, deserves some comments. First, note that $S_i \ge 0$, so that oil can only raise up towards the surface. Assume that $p_i = \pi_i$ and $p_{i+1} = \pi_{i+1}$ with $\pi_i < \pi_{i+1}$, then $S_i = 0$ if $h_i \le \frac{\pi_{i+1} - \pi_i}{\varrho g}$, which is the predicted height of the reservoir in ray-tracing or invasion percolation algorithms. Hence formula (9) allows to reproduce oil trapping by capillary barriers.*

The system (7)–(9) has to be complemented with initial and boundary conditions. We assume that the initial heights are given:

$$h_i(0, \boldsymbol{x}) = h_i^0(\boldsymbol{x}), \qquad 1 \le i \le I, \ \boldsymbol{x} \in \mathcal{O}. \tag{10}$$

We have to consider lateral boundary conditions for $\boldsymbol{x} \in \partial\mathcal{O}$, a boundary condition on the bottom of domain Ω for $z = b_0$ and a boundary condition on top of the domain Ω for $z = b_I$. We assume no-flux boundary conditions cross the lateral boundary, i.e.,

$$\left(\frac{\kappa_i}{\mu_o} h_i \nabla (p_i + \varrho g (h_i - b_i)) \right) \cdot \boldsymbol{n}_{\mathcal{O}} = 0 \quad \text{on } \partial\mathcal{O}, \tag{11}$$

where $\boldsymbol{n}_{\mathcal{O}}$ denotes the normal to $\partial\mathcal{O}$ outward w.r.t. $\mathcal{O}$. Imposing top and bottom boundary conditions are needed to prescribe the extremal fluxes S_0 and S_I. In order to simplify the stability analysis of the Finite Volume scheme carried out in Section 3.3, we will assume that the system is isolated, i.e.,

$$S_0(t, \boldsymbol{x}) = S_I(t, \boldsymbol{x}) = 0, \qquad t \ge 0, \ \boldsymbol{x} \in \mathcal{O}. \tag{12}$$

but other boundary conditions will be used in the numerical simulations.

1.2.4. *Energy stability of the model.* The goal of this section is to show that our reduced model preserves an important feature of Darcean immiscible incompressible two-phase flows, namely the decay of the energy along time [6, 7].

Denote by $\boldsymbol{h} = (h_i)_{1 \le i \le I}$ and $\boldsymbol{p} = (p_i)_{1 \le i \le I}$. The energy functional corresponding to the reduced model (7)–(12) writes

$$\mathfrak{E}(\boldsymbol{h}) = \sum_{i=1}^{I} \int_{\mathcal{O}} \left(\pi_i h_i + \frac{1}{2} \varrho g \left(b_i - h_i \right)^2 \right) \phi_i \mathrm{d}\boldsymbol{x}. \tag{13}$$

Proposition 1.2. *Let $(\boldsymbol{h}, \boldsymbol{p})$ be a smooth solution to (7)–(12) then*

$$\frac{\mathrm{d}}{\mathrm{d}t} \mathfrak{E}(\boldsymbol{h}) \le 0.$$

Proof. Multiplying equation (8) by $p_i + \varrho g (h_i - b_i)$, integrating over $\mathcal{O}$ and summing over i yields

$$A + B + C = 0,$$

where, using the boundary conditions (11) and (12), we have set

$$A = \sum_{i=1}^{I} \int_{\mathcal{O}} \partial_t h_i \left(p_i + \varrho g(h_i - b_i)\right) \phi_i \mathrm{d}\boldsymbol{x},$$
$$B = \sum_{i=1}^{I} \int_{\mathcal{O}} \frac{\kappa_i}{\mu_{\mathrm{o}}} h_i \left|\nabla \left(p_i + \varrho g(h_i - b_i)\right)\right|^2 \mathrm{d}\boldsymbol{x},$$
$$C = \sum_{i=1}^{I-1} \int_{\mathcal{O}} S_i \left(p_i - p_{i+1} + \varrho g \left(h_i - h_{i+1} - (b_i - b_{i+1})\right)\right) \mathrm{d}\boldsymbol{x}.$$

In view of relation (7), either $\partial_t h_i = 0$ or $p_i = \pi_i$, hence $A = \frac{\mathrm{d}}{\mathrm{d}t}\mathfrak{E}(\boldsymbol{h})$. Since $B \geq 0$, it only remains to check that $C \geq 0$ to conclude the proof. It follows from the definition (9) of S_i that

$$C = \sum_{i=1}^{I-1} \int_{\mathcal{O}} \frac{\kappa_i}{\mu_w \frac{\kappa_{i+1}}{\kappa_i} H_{i+1} + \mu_o h_i} \Big(\left(\varrho g h_i - (p_{i+1} - p_i)\right)^+ \Big)^2 \mathrm{d}\boldsymbol{x} + \sum_{i=1}^{I-1} \int_{\mathcal{O}} S_i (b_{i+1} - b_i - h_{i+1}).$$

The first term in the right-hand side is obviously non-negative, as well as the second term since $h_{i+1} \leq H_{i+1} = b_{i+1} - b_i$ and $S_i \geq 0$. □

Proposition 1.2 shows that $\mathfrak{E}(\boldsymbol{h})$ is a Lyapunov functional for our model. We will pay attention in Section 3 to propose a Finite Volume scheme that preserves this property at the discrete level.

2. Derivation of the reduced model

The goal of this section is the formal justification of model (7)–(9). This will be done starting from a well-established Darcean model for immiscible incompressible two-phase flows.

2.1. Starting from a full Darcean model.

Our starting point is a classical incompressible immiscible two-phase flow problem

$$\phi_i \partial_t s_{\mathrm{o}} + \nabla_{(\boldsymbol{x},z)} \cdot \boldsymbol{v}_{\mathrm{o}} = 0 \quad \text{in } \mathbb{R}_+ \times \Omega_i,\ i \in \{1, \dots, I\}, \tag{14}$$

where the filtration velocity $\boldsymbol{v}_{\mathrm{o}}$ is related to the oil pressure through the Darcy-Muskat law

$$\boldsymbol{v}_\alpha = -\frac{k_{\alpha,i}(s_\alpha)}{\mu_\alpha} \kappa_i \nabla_{(\boldsymbol{x},z)} \left(p_\alpha + \varrho_\alpha g z\right), \qquad \alpha \in \{\mathrm{o}, \mathrm{w}\}. \tag{15}$$

In the two above formulas (14)–(15), we denoted the $(d+1)$ dimensional differential divergence and gradient by $\nabla_{(\boldsymbol{x},z)}\cdot$ and $\nabla_{(\boldsymbol{x},z)}$ in order to stress the difference with the d-dimensional operators ∇ and $\nabla\cdot$ used in the reduced model (8). The water pressure is assumed to be hydrostatic in the whole Ω, i.e., (2) holds. The relative permeability functions $k_{\mathrm{o},i}$ are nondecreasing and satisfy $k_{\mathrm{o},i}(0) = 0$, $k_{\mathrm{o},i}(1) = 1$. Finally, the problem is closed by thanks to a capillary pressure relation with capillary pressures depending essentially not on the saturation but only on the layer i: the porous media are assumed to be infinitely poorly graded [1]. Following

the previous works of [24, 4, 5, 8], the capillary pressure function is extended into a maximal monotone graph, leading to

$$p_{\rm o} - p_{\rm w} \in \check{\pi}_i(s_{\rm o}) \quad \text{in } \mathbb{R}_+ \times \Omega_i, \tag{16}$$

where

$$\check{\pi}_i(s) = \begin{cases} (-\infty, \pi_i] & \text{if } s = 0, \\ \pi_i & \text{if } 0 < s < 1, \\ [\pi_i, +\infty) & \text{if } s = 1, \end{cases} \tag{17}$$

for some constant $\pi_i \in \mathbb{R}$.

Using (2) and (16), Eq. (14) reduces to the Hele-Shaw type problem

$$\phi_i \partial_t s_{\rm o} - \nabla_{(\boldsymbol{x},z)} \cdot \left(\frac{k_{{\rm o},i}(s_{\rm o})}{\mu_{\rm o}} \kappa_i \nabla_{(\boldsymbol{x},z)} \left(\zeta + (\varrho_{\rm o} - \varrho_{\rm w}) g z \right) \right) = 0 \quad \text{in } \mathbb{R}_+ \times \Omega_i,$$

with $\zeta(t, \boldsymbol{x}, z) \in \check{\pi}_i(s_{\rm o}(t, \boldsymbol{x}, z))$. The diffusion is degenerated so that one can reasonably assume that both phases are disjointed, i.e., $s_\alpha \in \{0, 1\}$ a.e. in $\mathbb{R}_+ \times \Omega$. Since $\varrho_{\rm o} < \varrho_{\rm w}$, it is expected that $s_{\rm o} = 1$ on top of the layers Ω_i, while $s_{\rm w} = 1$ in the bottom of the layers. We suppose that the two phases are separated by a sharp interface located at $z = \gamma_i(t, \boldsymbol{x}) \in [b_{i-1}(\boldsymbol{x}), b_i(\boldsymbol{x})]$. Denoting by

$$\Omega^t_{{\rm o},i} = \bigcup_{\boldsymbol{x} \in \mathcal{O}} \{\boldsymbol{x}\} \times (\gamma_i(t, \boldsymbol{x}), b_i(\boldsymbol{x})), \quad \text{and} \quad Q_{\rm o} = \bigcup_{t \in (0,T)} \left(\{t\} \times \bigcup_{1 \le i \le I} \Omega^t_{{\rm o},i} \right),$$

we assume that for all $t \ge 0$,

$$s_{\rm o}(t, \boldsymbol{x}, z) = \begin{cases} 1 & \text{if } (\boldsymbol{x}, z) \in \bigcup_{1 \le i \le I} \Omega^t_{{\rm o},i}, \\ 0 & \text{otherwise.} \end{cases} \tag{18}$$

and that the oil pressure is hydrostatic in $Q_{\rm o}$, i.e.,

$$p_{\rm o}(t, \boldsymbol{x}, z) = -\varrho_{\rm o} g z + C_i(t, \boldsymbol{x}), \quad \forall t \in \mathbb{R}_+, \ \forall (\boldsymbol{x}, z) \in \Omega^t_{{\rm o},i}. \tag{19}$$

The ansatz (18)–(19) together with hydrostatic water pressure (2) and mainly horizontal interfaces b_i are at the basis of the derivation of the Dupuit approximation to be described in the next section.

2.2. **Derivation of the vertically integrated equations.** We focus now on the derivation of vertically integrated equations for the evolution of the oil heights h_i. For the sake of simplicity, we do not detail the formal asymptotics that lead to our model (as for instance in [16]), and we rather just base our presentation on the ansatz (18)–(19).

We are interested in the evolution of the interfaces $\gamma_i(t, \boldsymbol{x})$. The ansatz about the strong separation of the oil and water phases in each layer detailed above yields

$$h_i(t, \boldsymbol{x}) = b_i(\boldsymbol{x}) - \gamma_i(t, \boldsymbol{x}) = \int_{b_{i-1}(\boldsymbol{x})}^{b_i(\boldsymbol{x})} s_{\rm o}(t, \boldsymbol{x}, z) {\rm d}z, \quad \forall (t, \boldsymbol{x}) \in \mathbb{R}_+ \times \mathcal{O}.$$

Therefore, using (14), we obtain that

$$\phi_i \partial_t \gamma_i = -\phi_i \partial_t h_i = -\int_{b_{i-1}}^{b_i} \phi_i \partial_t s_{\rm o}(t, \boldsymbol{x}, z) {\rm d}z = \int_{b_{i-1}}^{b_i} \nabla_{(\boldsymbol{x},z)} \cdot \boldsymbol{v}_{\rm o} {\rm d}z.$$

Since $s_{\rm o}(t,\boldsymbol{x},z)=0$ if $z\in(b_{i-1}(\boldsymbol{x}),\gamma_i(t,\boldsymbol{x}))$ and since $k_{{\rm o},i}(0)=0$, it follows from (15) that $\boldsymbol{v}_{\rm o}(t,\boldsymbol{x},z)=\boldsymbol{0}$, then it is in particular divergence free. Therefore, one can rewrite

$$-\phi_i\partial_t h_i=\int_{\gamma_i(t,\boldsymbol{x})}^{b_i(\boldsymbol{x})}\nabla_{(\boldsymbol{x},z)}\cdot\boldsymbol{v}_{\rm o}(t,\boldsymbol{x},z){\rm d}z.$$

Splitting the oil velocity $\boldsymbol{v}_{\rm o}$ into its horizontal part $\boldsymbol{v}_{\rm o}^{\boldsymbol{x}}$ and its vertical part $v_{\rm o}^z\boldsymbol{e}_z$, we get that

$$\phi_i\partial_t\gamma_i(t,\boldsymbol{x})=\int_{\gamma_i(t,\boldsymbol{x})}^{b_i(\boldsymbol{x})}\nabla\cdot\boldsymbol{v}_{\rm o}^{\boldsymbol{x}}(t,\boldsymbol{x},z){\rm d}z+v_{\rm o}^z(t,\boldsymbol{x},b_i(\boldsymbol{x}))-v_{\rm o}^z(t,\boldsymbol{x},\gamma_i(t,\boldsymbol{x})).\tag{20}$$

In the case where b_i varies slowly (i.e., if the interface is mainly horizontal), then the quantity $v_{\rm o}^z(t,\boldsymbol{x},b_i(\boldsymbol{x}))$ can be seen as a the flux of oil leaking from Ω_i to Ω_{i+1} that we denote by $S_i(t,\boldsymbol{x})$ in what follows. The obtention of a closure relation between for S_i is the purpose of the forthcoming Section 2.3.

It appears that

$$\boldsymbol{v}_{\rm o}^{\boldsymbol{x}}(t,\boldsymbol{x},z)=-\frac{\kappa_i}{\mu_{\rm o}}\nabla p_{\rm o}(t,\boldsymbol{x},z)$$

is constant w.r.t. $z\in(b_{i-1}(\boldsymbol{x}),\gamma_i(t,\boldsymbol{x}))$ where $s_{\rm o}=1$ — thus so does $\nabla\cdot\boldsymbol{v}_{\rm o}^{\boldsymbol{x}}(t,\boldsymbol{x})$ — since, thanks to (15) and (19),

$$\partial_z\boldsymbol{v}_{\rm o}^{\boldsymbol{x}}(t,\boldsymbol{x},z)=-\frac{\kappa_i}{\mu_{\rm o}}\nabla\partial_z p_{\rm o}(t,\boldsymbol{x},z)=\frac{\kappa_i}{\mu_{\rm o}}\nabla\varrho_o g=0.$$

Therefore, we obtain

$$\begin{aligned}\int_{\gamma_i(t,\boldsymbol{x})}^{b_i(\boldsymbol{x})}\nabla\cdot\boldsymbol{v}_{\rm o}^{\boldsymbol{x}}(t,\boldsymbol{x}){\rm d}z&=\nabla\cdot\int_{\gamma_i(t,\boldsymbol{x})}^{b_i(\boldsymbol{x})}\boldsymbol{v}_{\rm o}^{\boldsymbol{x}}(t,\boldsymbol{x}){\rm d}z+\boldsymbol{v}_{\rm o}^{\boldsymbol{x}}(t,\boldsymbol{x})\cdot\nabla(\gamma_i(t,\boldsymbol{x})-b_i(\boldsymbol{x}))\\&=-\nabla\cdot\left(\frac{\kappa_i}{\mu_{\rm o}}h_i(t,\boldsymbol{x})\nabla p_o(t,\boldsymbol{x})\right)+\boldsymbol{v}_{\rm o}^{\boldsymbol{x}}(t,\boldsymbol{x})\cdot\nabla(\gamma_i(t,\boldsymbol{x})-b_i(\boldsymbol{x})).\end{aligned}$$

The vectors $\boldsymbol{n}_{b_i}=\begin{pmatrix}-\nabla b_i\\1\end{pmatrix}$ and $\boldsymbol{n}_{\gamma_i}=\begin{pmatrix}-\nabla\gamma_i\\1\end{pmatrix}$ are orthogonal to the hypersurfaces $\{(\boldsymbol{x},b_i(\boldsymbol{x})),\ \boldsymbol{x}\in\mathcal{O}\}$ and $\{(\boldsymbol{x},\gamma_i(t,\boldsymbol{x})),\ \boldsymbol{x}\in\mathcal{O}\}$ respectively. Equation (20) rewrites

$$\phi_i\partial_t h_i-\nabla\cdot\left(\frac{\kappa_i}{\mu_{\rm o}}h_i\nabla p_o\right)=\boldsymbol{v}_{\rm o}\cdot(\boldsymbol{n}_{\gamma_i}-\boldsymbol{n}_{b_i}).\tag{21}$$

As a consequence of (16)–(17), the capillary pressure p_o-p_w in Ω_i is greater than π_i if $s_{\rm o}=1$ and smaller than π_i if $s_{\rm o}=0$. Then capillary pressure is equal to π_i at the interface between the two phases provided this interface is inside Ω_i:

$$p_{\rm o}(t,\boldsymbol{x},\gamma_i(t,\boldsymbol{x}))-p_{\rm w}(t,\boldsymbol{x},\gamma_i(t,\boldsymbol{x}))=\pi_i,\quad\forall(t,\boldsymbol{x})\text{ s.t. }b_{i-1}(\boldsymbol{x})<\gamma_i(t,\boldsymbol{x})<b_i(\boldsymbol{x}).\tag{22}$$

In the case where $\gamma_i(t,\boldsymbol{x})=b_i(\boldsymbol{x})$, meaning that there is no oil in the column $\{\boldsymbol{x}\}\times(b_{i-1}(\boldsymbol{x}),b_i(\boldsymbol{x}))$ at time t, then (16)–(17) leads to

$$p_{\rm o}(t,\boldsymbol{x},\gamma_i(t,\boldsymbol{x}))-p_{\rm w}(t,\boldsymbol{x},\gamma_i(t,\boldsymbol{x}))\le\pi_i\quad\forall(t,\boldsymbol{x})\text{ s.t. }h_i(t,\boldsymbol{x})=0.\tag{23}$$

Let $\boldsymbol{x}\in\mathcal{O}$, then assume that the $\gamma_i(\boldsymbol{x})\in(b_{i-1}(\boldsymbol{x}),b_i(\boldsymbol{x}))$. Similarly, if $\gamma_i(t,\boldsymbol{x})=b_{i-1}(\boldsymbol{x})$, one obtains

$$p_{\rm o}(t,\boldsymbol{x},\gamma_i(t,\boldsymbol{x}))-p_{\rm w}(t,\boldsymbol{x},\gamma_i(t,\boldsymbol{x}))\ge\pi_i,\quad\forall(t,\boldsymbol{x})\text{ s.t. }h_i(t,\boldsymbol{x})=H_i(\boldsymbol{x}).\tag{24}$$

The relations (22)–(24) can be summarized in the compact form

$$p_{\rm o}(t,\boldsymbol{x},\gamma_i(t,\boldsymbol{x}))-p_{\rm w}(t,\boldsymbol{x},\gamma_i(t,\boldsymbol{x}))\in\widetilde{\pi}_i(\boldsymbol{x},h_i(t,\boldsymbol{x})),$$

where $\widetilde{\pi}_i(\boldsymbol{x},\cdot)$ is the maximal monotone graph defined by (6).

Let $t \geq 0$, $\boldsymbol{x} \in \mathcal{O}$ and let $z \in (\gamma_i(t,\boldsymbol{x}), b_i(\boldsymbol{x}))$, then thanks to (19), one has

$$\begin{aligned} p_{\mathrm{o}}(t,\boldsymbol{x},z) =& p_{\mathrm{o}}(t,\boldsymbol{x},\gamma_i(t,\boldsymbol{x})) - (z-\gamma_i(t,\boldsymbol{x}))\varrho_{\mathrm{o}} g \\ =& p_{\mathrm{w}}(t,\boldsymbol{x},\gamma_i(t,\boldsymbol{x})) + p_i(t,\boldsymbol{x}) - (z-\gamma_i(t,\boldsymbol{x}))\varrho_{\mathrm{o}} g \end{aligned}$$

for some $p_i(t,\boldsymbol{x}) \in \widetilde{\pi}_i(\boldsymbol{x}, h_i(t,\boldsymbol{x}))$. Using the expression (2) of the water pressure, one gets

$$p_{\mathrm{o}}(t,\boldsymbol{x},z) = p_i(t,\boldsymbol{x}) + (\varrho_{\mathrm{w}} - \varrho_{\mathrm{o}}) g (h_i(t,\boldsymbol{x}) - b_i(\boldsymbol{x})) - \varrho_{\mathrm{o}} g z$$

for all $z \in (\gamma_i(t,\boldsymbol{x}), b_i(\boldsymbol{x}))$. In particular, we obtain the

$$\nabla p_{\mathrm{o}} = \nabla \left(p_i + \varrho g (h_i - b_i) \right) \quad \text{on } \Omega^t_{\mathrm{o},i}. \tag{25}$$

Using (25) in (21) yields

$$\phi_i \partial_t h_i - \nabla \cdot \left(\frac{\kappa_i}{\mu_{\mathrm{o}}} h_i \nabla \left(p_i + \varrho g (h_i - b_i) \right) \right) = \boldsymbol{v}_{\mathrm{o}} \cdot (\boldsymbol{n}_{\gamma_i} - \boldsymbol{n}_{b_i}) \,. \tag{26}$$

We have recovered the left-hand side of (8).

Concerning the right-hand side appearing in (26), the term $S_i := \boldsymbol{v}_{\mathrm{o}} \cdot \boldsymbol{n}_{b_i}$ shall be interpreted as the oil flux between Ω_i and Ω_{i+1} leaving $\Omega^t_{\mathrm{o},i}$ from above, whereas $\boldsymbol{v}_{\mathrm{o}} \cdot \boldsymbol{n}_{\gamma_i}$ correspond to the oil flux entering $\Omega^t_{\mathrm{o},i}$ from below. For simplicity, we assume that

$$\boldsymbol{v}_{\mathrm{o}}(t,\boldsymbol{x}) \cdot \boldsymbol{n}_{\gamma_i}(t,\boldsymbol{x}) = S_{i-1}(t,\boldsymbol{x}),$$

neglecting the delay corresponding to the time oil needs to reach γ_i from b_{i-1}. This completes the derivation of (8). Our next section is devoted to the derivation of the closure relation (9).

2.3. **Flux exchange term S_i between two layers.** The formula (9) for the interlayer fluxes relies on a purely one-dimensional study in the vertical direction.

We first need to relax the assumption on hydrostatic phase pressures (2) and (19) since it implies through (15) that the vertical component of $\boldsymbol{v}_{\mathrm{o}}$ is zero. We still assume that $z \mapsto p_{\mathrm{o}}(t,\boldsymbol{x},z)$ and $z \mapsto p_{\mathrm{w}}(t,\boldsymbol{x},z)$ are piecewise affine, but rather than looking for hydrostatic profiles, we look for profiles for which the capillary pressure remains constant equal to $p_i \in \widetilde{\pi}_i(\boldsymbol{x}, h_i(t,\boldsymbol{x}))$ for $z \in (\gamma_i(t,\boldsymbol{x}), b_i(\boldsymbol{x}))$, i.e.,

$$\begin{cases} p_{\mathrm{w}}(t,\boldsymbol{x},z) = (\alpha_i(t,\boldsymbol{x}) - \varrho_{\mathrm{o}} g)\,(z - b_i(\boldsymbol{x})) + \beta_i(t,\boldsymbol{x}), \\ p_{\mathrm{o}}(t,\boldsymbol{x},z) = p_i + (\alpha_i(t,\boldsymbol{x}) - \varrho_{\mathrm{o}} g)\,(z - b_i(\boldsymbol{x})) + \beta_i(t,\boldsymbol{x}). \end{cases}$$

Above the interface b_i, we also assume a linear profile of both phase pressures:

$$\begin{cases} p_{\mathrm{w}}(z) = (\alpha_{i+1} - \varrho_{\mathrm{w}} g)(z - b_i) + \beta_{i+1}, \\ p_{\mathrm{o}}(z) = p_{i+1} + (\alpha_{i+1} - \varrho_{\mathrm{w}} g)(z - b_i) + \beta_{i+1}, \end{cases} \qquad z \in (b_i, b_{i+1}),$$

where $p_{i+1}(t,\boldsymbol{x}) \in \widetilde{\pi}_{i+1}(\boldsymbol{x}, h_{i+1}(t,\boldsymbol{x}))$. The continuity of the oil pressure at $z = b_i(\boldsymbol{x})$ writes

$$p_i + \beta_i = p_{i+1} + \beta_{i+1}. \tag{27}$$

The total flux $\boldsymbol{v}_{\mathrm{o}} + \boldsymbol{v}_{\mathrm{w}}$ is divergence free. We assume that its vertical contribution is equilibrated, i.e., $v^z_{\mathrm{o}} + v^z_{\mathrm{w}}$ does not depend on z. As a consequence of the Darcy-Muskat law (15), and since $s_{\mathrm{o}} \approx 1$ (resp. $s_{\mathrm{o}} \approx 0$) below (resp. above) the interface

b_i, the total flux $v_{\rm o}^z + v_{\rm w}^z$ is mainly equal $v_{\rm o}^z$ (resp. $v_{\rm w}^z$) below (resp. above) the interface. The continuity of the total flux across the interface then yields

$$-\frac{\kappa_i}{\mu_{\rm o}}\alpha_i = -\frac{\kappa_{i+1}}{\mu_{\rm w}}\alpha_{i+1}. \tag{28}$$

Two additional equations are needed. They are obtained by fitting the non-hydrostatic water pressure with hydrostatic profiles at $z = b_{i+1}(\boldsymbol{x})$ and $z = \gamma_i(t,\boldsymbol{x})$. This leads respectively to the relations

$$\alpha_{i+1}H_{i+1} + \beta_{i+1} = -\varrho_{\rm w} g b_i, \tag{29}$$

$$-\alpha_i h_i + \beta_i = -\varrho_{\rm w} g b_i + \varrho g h_i. \tag{30}$$

The system (27)–(30) admits a unique solution $(\alpha_i, \alpha_{i+1}, \beta_i, \beta_{i+1})^T$ for any non-negative h_i and positive H_{i+1}, and yields

$$\alpha_i = \frac{1}{h_i + \frac{\mu_{\rm w}\kappa_i}{\mu_{\rm o}\kappa_{i+1}}H_{i+1}}\left(p_{i+1} - p_i - \varrho g h_i\right).$$

Now, it remains to notice that since the flow is driven by buoyancy, the oil flux S_i is always non-negative. When positive, it is given by

$$S_i(t,\boldsymbol{x}) = -\frac{\kappa_i}{\mu_{\rm o}}(\partial_z p_{\rm o}(t,\boldsymbol{x},b_i(\boldsymbol{x})^-) + \varrho_{\rm o} g) = -\frac{\kappa_i}{\mu_{\rm o}}\alpha_i, \tag{31}$$

where $\partial_z p_{\rm o}(t,\boldsymbol{x},b_i(\boldsymbol{x})^-)$ denotes the left derivative at $z = b_i$ of the piecewise affine function $z \mapsto p_{\rm o}(t,\boldsymbol{x},z)$. If the formula (31) provides a negative value, then $S_i(t,\boldsymbol{x})$ is set to 0, leading to Formula (9).

3. Finite Volume approximation

3.1. **A two-point flux approximation Finite Volume scheme.** We propose now Finite Volume scheme to approximate the solutions to problem (7)–(12). The equation (8) is of degenerate parabolic-elliptic type. We propose to discretize it thanks to a two-point flux approximation with upstream mobility. Since we use a two-point flux approximation of the diffusive flux, the mesh has to fulfil a so-called orthogonality condition (see [12] or [11]). Details on the discretization of the domain are presented in the next section.

3.1.1. *Discretization of* $\mathbb{R}_+ \times \Omega$. Before discretizing the time domain, we focus on the spatial domain. Taking advantage of the structure (1) of Ω, we mainly have to mesh $\mathcal{O}$. In what follows, $\mathcal{O}$ is assumed to be polygonal if $d = 2$. We use standard notations from [12].

An admissible discretization of $\mathcal{O}$ is made of a family of convex polygonal control volumes (or cells) $\mathcal{T}$, a family of edges $\mathcal{E}$ and a family of cell centers $(\boldsymbol{x}_K)_{K\in\mathcal{T}}$. The boundary of the control volumes are made of edges. More precisely, for all $K \in \mathcal{T}$, there exists a subset $\mathcal{E}_K$ of $\mathcal{E}$ such that $\partial K = \bigcup_{\sigma\in\mathcal{E}_K}\overline{\sigma}$. Moreover, we assume that $\mathcal{E} = \bigcup_{K\in\mathcal{T}}\mathcal{E}_K$. We assume that the control volumes mesh the whole d-dimensional domain $\mathcal{O}$, i.e., $\bigcup_{K\in\mathcal{T}}\overline{K} = \overline{\mathcal{O}}$, and that they are disjointed, i.e., $K \cap L = \emptyset$ if $K, L \in \mathcal{T}$ with $K \neq L$. More precisely, if $d = 2$, given two distinct control volumes K and L in $\mathcal{T}$, either the either 1-dimensional Lebesgue measure of $\overline{K} \cap \overline{L}$ is equal to 0, or there exists $\sigma \in \mathcal{E}$ such that $\overline{K} \cap \overline{L} = \overline{\sigma}$. If $d = 1$, then the edges reduce to points and $\overline{K} \cap \overline{L}$ is either empty or it reduces to some $\sigma \in \mathcal{E}$. Finally, given two neighbouring cells K and L sharing an edge σ, then we assume that the straight line joining $\boldsymbol{x}_K$ to $\boldsymbol{x}_L$ is orthogonal to σ and oriented in

the same sense as the normal to σ outward w.r.t. K. Finally, we decompose the set $\mathcal{E}$ of the edges into boundary edges $\mathcal{E}_{\rm ext} = \{\sigma \in \mathcal{E} \mid \sigma \subset \partial\mathcal{O}\}$ and internal edges $\mathcal{E}_{\rm int} = \{\sigma \in \mathcal{E} \mid \overline{\sigma} = \overline{K} \cap \overline{L} \text{ for some } K, L \in \mathcal{T}\}$. An internal edge $\sigma \in \mathcal{E}_{\rm int}$ between two cells K and L is denoted by $K|L$.

For all $K \in \mathcal{T}$, we denote by m_K the d-dimensional Lebesgue measure of K, while m_σ denotes the $(d-1)$-dimensional Lebesgue measure of the edge $\sigma \in \mathcal{E}$. For $\sigma = K|L$, we denote the transmissivity of σ by $\tau_\sigma = \frac{m_\sigma}{|\boldsymbol{x}_K - \boldsymbol{x}_L|}$.

For all $K \in \mathcal{T}$ and all $i \in \{0, \dots, I\}$, we denote by $b_{i,K} = \frac{1}{m_K} \int_K b_i(\boldsymbol{x}) \mathrm{d}\boldsymbol{x}$, and by $H_{i,K} = b_{i,K} - b_{i-1,K}$ for $i \in \{1, \dots, I\}$ the height of the $i^{\rm th}$ layer in the column corresponding to the cell K.

Concerning time, we consider an increasing sequence $(t_n)_{n\geq 0}$ with $t_0 = 0$ and $\lim_{n\to\infty} t_n = +\infty$. We denote by $\Delta t_n = t_n - t_{n-1}$ for $n \geq 1$.

3.1.2. *A time implicit finite volume scheme.* We will now present the discretization of the system (7)–(12).

Let us first discretize the initial condition (10) by

$$h^0_{i,K} = \frac{1}{m_K} \int_K h^0_i(\boldsymbol{x}) \mathrm{d}\boldsymbol{x}, \qquad K \in \mathcal{T},\ 1 \leq i \leq I. \tag{32}$$

At each time step $n \geq 1$, we seek oil heights and capillary pressures $\left(h^n_{i,K}, p^n_{i,K}\right)_{i,K}$ that are linked by the discrete counterpart to (7), namely

$$p^n_{i,K} \in \widetilde{\pi}_{i,K}(h^n_{i,K}), \tag{33}$$

where

$$\widetilde{\pi}_{i,K}(h) = \begin{cases} \pi_i & \text{if } 0 < h < H_{i,K}, \\ (-\infty, \pi_i] & \text{if } h = 0, \\ [\pi_i, +\infty) & \text{if } h = H_{i,K}. \end{cases} \tag{34}$$

They have to solve the discrete version of (8), that is

$$\begin{aligned} &\phi_i \frac{h^n_{i,K} - h^{n-1}_{i,K}}{\Delta t_n} m_K \\ &\quad + \sum_{\sigma = K|L} \tau_\sigma \frac{\kappa_i}{\mu_{\rm o}} h^n_{i,\sigma} \left(p^n_{i,K} - p^n_{i,L} + \varrho g (h^n_{i,K} - h^n_{i,L} - b_{i,K} + b_{i,L})\right) \\ &\qquad\qquad = \left(S^n_{i-1,K} - S^n_{i,K}\right) m_K. \end{aligned} \tag{35}$$

In (35), we used upwinding for the mobility: for all $\sigma = K|L \in \mathcal{E}_{\rm int}$,

$$h^n_{i,\sigma} = \begin{cases} h^n_{i,K} & \text{if } p^n_{i,K} + \varrho g (h^n_{i,K} - b_{i,K}) \geq p^n_{i,L} + \varrho g (h^n_{i,L} - b_{i,L}), \\ h^n_{i,L} & \text{otherwise.} \end{cases} \tag{36}$$

Note that there is no term corresponding to lateral fluxes in the second term of (35) as a consequence of (11).

Concerning the exchange terms between the layers, one sets

$$S^n_{i,K} = \frac{\kappa_i}{\mu_w \frac{\kappa_i}{\kappa_{i+1}} H_{i+1,K} + \mu_o h^n_{i,K}} \left(\varrho g h^n_{i,K} - (p^n_{i+1,K} - p^n_{i,K})\right)^+ \tag{37}$$

for $i \in \{1, \dots I-1\}$ and $K \in \mathcal{T}$ in accordance with (9), while

$$S^n_{0,K} = S^n_{I,K} = 0, \qquad K \in \mathcal{T}, \tag{38}$$

as suggested by (12).

Given a solution $\left(h_{i,K}^n, p_{i,K}^n\right)_{i,K}$ to the scheme (33)–(38) — the existence of such a solution is the purpose of Theorem 3.3 —, we define $\boldsymbol{h}^n = \left(h_{i,K}^n\right)_{i,K}$ and $\boldsymbol{p}^n = \left(p_{i,K}^n\right)_{i,K}$. We also reconstruct a piecewise constant in time and space approximate solution $(\boldsymbol{h}_{\mathcal{D}}, \boldsymbol{p}_{\mathcal{D}})$ defined by

$$h_{i,\mathcal{D}}^n(\boldsymbol{x}) = h_{i,K}^n \text{ and } p_{i,\mathcal{D}}^n(\boldsymbol{x}) = p_{i,K}^n \text{ if } \boldsymbol{x} \in K, \tag{39}$$

and then by $\boldsymbol{h}_{\mathcal{D}}^n = \left(h_{i,\mathcal{D}}^n\right)_{1\le i\le I}$ and $\boldsymbol{p}_{\mathcal{D}}^n = \left(p_{i,\mathcal{D}}^n\right)_{1\le i\le I}$.

3.2. **Auxiliary pressure and parametrization.** Solving directly the non-linear system (33)–(38) may be difficult. One cannot directly use Newton's method because of the degeneracy of the graphs $\widetilde{\pi}_{i,K}$. One solution to overpass this difficulty is to use variable switch [10] between $\boldsymbol{h}^n$ and $\boldsymbol{p}^n$. The formalism we adopt here is inspired from [2, 3]. It can be seen as a generalization of the variable switch even though its practical implementation is rather different.

Given $K \in \mathcal{T}$ and $i \in \{1, \dots, N\}$, the monotone graph $\widetilde{\pi}_{i,K}$ defined by (34) can be parametrized by two non-decreasing and Lipschitz continuous functions $\overline{h}_{i,K}$ and $\overline{p}_{i,K}$ in the sense that

$$p \in \widetilde{\pi}_{i,K}(h) \text{ iff there exists } u \in \mathbb{R} \text{ s.t. } h = \overline{h}_{i,K}(u) \text{ and } p = \overline{p}_{i,K}(u). \tag{40}$$

There are infinitely many functions $\overline{h}_{i,K}$ and $\overline{p}_{i,K}$ satisfying (40). One way to construct such functions is to use curvilinear coordinates along the graph $\widetilde{\pi}_{i,K}$. In what follows, we use the definitions

$$\overline{h}_{i,K}(u) = \begin{cases} 0 & \text{if } u \le \pi_i, \\ \frac{1}{\varrho g}(u - \pi_i) & \text{if } u \in [\pi_i, \pi_i + \varrho g H_{i,K}], \\ H_{i,K} & \text{if } u \ge \pi_i + \varrho g H_{i,K}, \end{cases} \tag{41a}$$

$$\overline{p}_{i,K}(u) = \begin{cases} u & \text{if } u \le \pi_i, \\ \pi_i & \text{if } u \in [\pi_i, \pi_i + \varrho g H_{i,K}], \\ u - \varrho g H_{i,K} & \text{if } u \ge \pi_i + \varrho g H_{i,K}. \end{cases} \tag{41b}$$

so that

$$\varrho g \overline{h}_{i,K}(u) + \overline{p}_{i,K}(u) = u, \qquad \forall u \in \mathbb{R}. \tag{42}$$

With this particular choice, the quantity $u_{i,K}^n$ such that $h_{i,K}^n = \overline{h}_{i,K}(u_{i,K}^n)$ and $p_{i,K}^n = \overline{p}_{i,K}(u_{i,K}^n)$ can be interpreted as the capillary pressure just below the interface $b_{i,K}^n$. We depict functions $\overline{h}_{i,K}$ and $\overline{p}_{i,K}$ defined by (41) corresponding to some graph $\widetilde{\pi}_{i,K}$ on Figure 3.

Given $\boldsymbol{h}^{n-1}$ such that $0 \le h_{i,K}^{n-1} \le H_{i,K}$, the numerical scheme then amounts to find $\boldsymbol{u}^n = \left(u_{i,K}^n\right)_{i,K}$ such that, for all $i \in \{1, \dots, I\}$ and all $K \in \mathcal{T}$, one has

$$\begin{aligned} &\phi_i \frac{\overline{h}_{i,K}(u_{i,K}^n) - h_{i,K}^{n-1}}{\Delta t_n} m_K \\ &\quad + \sum_{\sigma = K|L} \tau_\sigma \frac{\kappa_i}{\mu_{\mathrm{o}}} h_{i,\sigma}^n \left(u_{i,K}^n - u_{i,L}^n - \varrho g (b_{i,K} - b_{i,L})\right) = \left(S_{i-1,K}^n - S_{i,K}^n\right) m_K, \end{aligned} \tag{43}$$

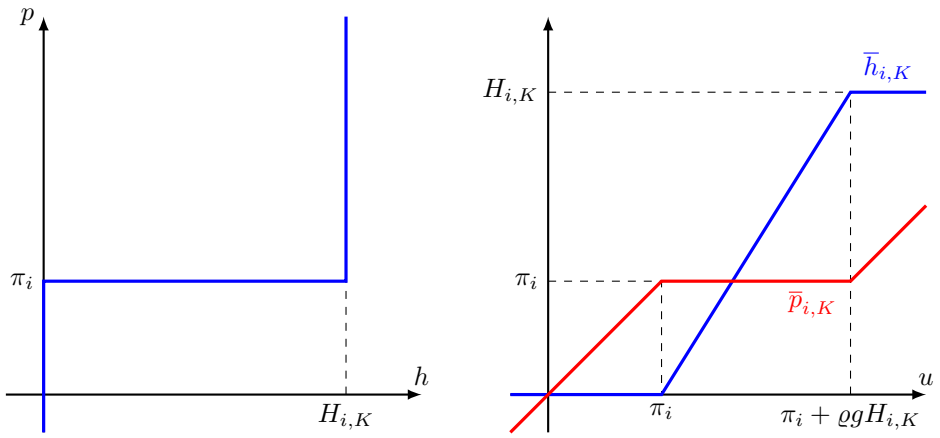

FIGURE 3. The maximal monotone graph $\widetilde{\pi}_{i,K}$ (left) can be parametrized in the sense of (40) by the functions $\overline{h}_{i,K}$ and $\overline{p}_{i,K}$ defined by (41) (right).

where, thanks to (42), the upstream mobility can be expressed as

$$h^n_{i,\sigma} = \begin{cases} h_{i,K}(u^n_{i,K}) & \text{if } u^n_{i,K} - \varrho g b_{i,K} \geq u^n_{i,L} - \varrho g b_{i,L}, \\ h_{i,L}(u^n_{i,L}) & \text{otherwise.} \end{cases} \tag{44}$$

The interlayer fluxes $S^n_{i,K}$ are discretized by

$$\begin{aligned} S^n_{i,K} &= \overline{S}_{i,K}(u^n_{i,K}, u^n_{i+1,K}) \\ &= \frac{\kappa_i}{\mu_w \frac{\kappa_{i+1}}{\kappa_i} H_{i+1,K} + \mu_o h_{i,K}(u^n_{i,K})} \Big(u^n_{i,K} - \overline{p}_{i+1,K}(u^n_{i+1,K}) \Big)^+ \end{aligned} \tag{45}$$

if $i \in \{1, \dots, I-1\}$, whereas we keep (38) for $i = 0$ or $i = I$. Once $\boldsymbol{u}^n$ has been computed, one can recover the physical quantities $\boldsymbol{h}^n$ and $\boldsymbol{p}^n$ by setting

$$h^n_{i,K} = \overline{h}_{i,K}(u^n_{i,K}) \quad \text{and} \quad p^n_{i,K} = \overline{p}_{i,K}(u^n_{i,K}), \qquad K \in \mathcal{T},\ i \in \{1, \dots, I\}. \tag{46}$$

In particular, the solution $(\boldsymbol{h}^n, \boldsymbol{p}^n) \in \left(\mathbb{R}^{I \times \#\mathcal{T}}\right)^2$ is fully characterized by the knowledge of $\boldsymbol{u}^n \in \mathbb{R}^{I \times \#\mathcal{T}}$.

3.3. **Stability analysis and existence of a discrete solution.** The main goal of this section is to show that the proposed scheme (43)–(46) is stable and that it admits (at least) one solution $\boldsymbol{u}^n$ at each time step $n \geq 1$.

Our first lemma concerns the conservation of mass. It is a straightforward consequence of the conservativity of the scheme and of the definition (32) of the initial data. Its proof is left to the reader.

Lemma 3.1 (Conservation of the oil mass)**.** *Let $\boldsymbol{u}^n$ be a solution to the scheme (43)–(45) and let $\boldsymbol{h}^n$ be given by (46), then*

$$\sum_{i=1}^{I} \sum_{K \in \mathcal{T}} m_K h^n_{i,K} = \sum_{i=1}^{I} \sum_{K \in \mathcal{T}} m_K h^{n-1}_{i,K} = \sum_{i=1}^{I} \int_{\mathcal{O}} h^0_i(\boldsymbol{x}) \mathrm{d}\boldsymbol{x}, \qquad \forall n \geq 1.$$

3.3.1. *Lack of uniqueness of the discrete solution* $\boldsymbol{u}^n$. Before dealing with the existence of a discrete solution $\boldsymbol{u}^n$, let us briefly discuss about the lack of uniqueness.

Assume that $u^n_{i,K} \le \pi_i$ for all i and all K, so that $\boldsymbol{h}^n = \boldsymbol{0}$. Because of the conservation of mass, one has necessarily $\boldsymbol{h}^{n-1} = \boldsymbol{0}$ too. Therefore, the two first terms in (43) vanish and $\boldsymbol{u}^n$ is a solution as soon as $S_{i,K}(u^n_{i,K}, u^n_{i+1,K}) = 0$ for all $i \in \{1, \dots, I-1\}$. This condition is fulfilled as soon as $u^n_{i,K} \le u^n_{i+1,K}$ for all $K \in \mathcal{T}$ and all $i \in \{1, \dots, I-1\}$, so that it is easy to construct various solutions $\boldsymbol{u}^n$ corresponding to the trivial configuration $\boldsymbol{h}^n = \boldsymbol{0}$.

Similarly, one can construct many solutions corresponding to the case $\boldsymbol{h}^n = \boldsymbol{h}^{n-1} = \boldsymbol{H} = (H_{i,K})_{i,K}$, requiring that $u^n_{i,K} \ge \pi_i + \varrho g H_{i,K}$. The horizontal fluxes vanish as soon as

$$u^n_{i,K} - \varrho g b_{i,K} = u^n_{i,L} - \varrho g b_{i,L} = C^n_i, \qquad \forall (K,L) \in \mathcal{T}^2.$$

The interlayer vertical fluxes $\left(S^n_{i,K}\right)_{i,K}$ vanish if

$$u^n_{i,K} \le \overline{p}_{i+1,K}(u^n_{i+1,K}) = u^n_{i+1,K} - \varrho g H_{i+1,K}, \qquad K \in \mathcal{T},\ 1 \le i \le I-1.$$

Here again, it is possible to construct several solutions $\boldsymbol{u}^n$ corresponding to the steady profile $\boldsymbol{h}^n = \boldsymbol{H}$.

3.3.2. *Existence of a discrete solution.* Our proof for the existence of a discrete solution is based on a topological degree argument [18, 9]. But in view of the degeneracy pointed out in Section 3.3.1, we have first add some stabilization terms to the scheme. To this end, define $b_\star = \min_K b_{0,K}$ and

$$\pi_\star = \min_{1 \le i \le I} \pi_i, \quad \text{and} \quad u^\star_{i,K} = \max_{1 \le j \le I} \pi_j + \varrho g (b_{i,K} - b_\star).$$

The stabilized scheme is obtained by replacing (43) by

$$\begin{aligned} (47) \quad & \phi_i \frac{\overline{h}_{i,K}(u^n_{i,K}) - h^{n-1}_{i,K}}{\Delta t_n} m_K - (\pi_\star - u^n_{i,K})^+ + (u^n_{i,K} - u^\star_{i,K})^+ \\ & + \sum_{\sigma = K|L} \tau_\sigma \frac{\kappa_i}{\mu_{\mathrm{o}}} h^n_{i,\sigma} \left(u^n_{i,K} - u^n_{i,L} - \varrho g (b_{i,K} - b_{i,L}) \right) = \left(S^n_{i-1,K} - S^n_{i,K} \right) m_K. \end{aligned}$$

The following lemma shows the solutions to the stabilized scheme (47) are also solution to the original scheme (43). Notice that any solution $\boldsymbol{u}^n$ to the stabilized scheme such that $\pi_\star \le u^n_{i,K} \le u^\star_{i,K}$.

Lemma 3.2 (Uniform estimate on $\boldsymbol{u}^n$)**.** *Let $\boldsymbol{u}^n$ be a solution to (47), (44) and (45), then*

$$\pi_\star \le u^n_{i,K} \le u^\star_{i,K}, \qquad K \in \mathcal{T},\ 1 \le i \le I.$$

Proof. Let us first focus on the lower bound. Let i_0, K_0 be such that $u^n_{i_0,K_0} = \min_{i,K} u^n_{i,K}$, and assume for contradiction that $u^n_{i_0,K_0} < \pi_\star$. Since $u^n_{i_0,K_0} \le \pi_{i+1}$, it follows from the definitions (41b) and (45) that $S^n_{i_0,K_0} = 0$. Moreover, since $h^n_{i_0,K_0} = 0$, it follows from the upwind choice (44) of the mobility that

$$\sum_{\sigma = K_0|L} \tau_\sigma \frac{\kappa_{i_0}}{\mu_{\mathrm{o}}} h^n_{i_0,\sigma} \left(u^n_{i_0,K_0} - u^n_{i_0,L} - \varrho g (b_{i_0,K_0} - b_{i_0,L}) \right) \le 0.$$

Therefore, the left-hand side of (47) is negative because of the stabilization term, whereas the right-hand side is nonnegative, providing the expected contradiction.

Let us now establish the upper bound with a similar strategy. To this end, assume that

$$i_1 = \min\left\{ i \in \{1,\dots,I\} \;\middle|\; \text{there exists } u^n_{i,K} > u^\star_{i,K} \right\} \tag{48}$$

is well defined, i.e., the set on which we minimize is not empty. Let K_1 be such that

$$u^n_{i_1,K_1} - \varrho g b_{i_1,K_1} \geq u^n_{i_1,L} - \varrho g b_{i_1,L}, \qquad \forall L \in \mathcal{T}.$$

This implies in particular, $u^n_{i_1,K_1} > u^\star_{i_1,K_1}$, so that

$$u^n_{i_1,K_1} - \varrho g (b_{i_1,K_1} - b_\star) > \max_j \pi_j \geq u^n_{i_1-1,K_1} - \varrho g (b_{i_1-1,K_1} - b_\star) \tag{49}$$

due to the definition of i_1. This yields in particular that

$$\overline{p}_{i_1,K_1}(u^n_{i_1,K_1}) = u^n_{i_1,K_1} - \varrho g H_{i_1,K_1} > u^n_{i_1-1,K_1},$$

hence $S^n_{i_1-1,K_1} = 0$. Since $b_{i_1,K_1} \geq b_\star + H_{i_1,K_1}$, we also deduce from (49) that $h^n_{i_1,K_1} = H_{i_1,K_1}$. Therefore, the left-hand side of (47) for $i = i_1$ and $K = K_1$ is positive because of the stabilization term, while the right-hand side is nonpositive. We get a contradiction, which implies that the minimization set in (48) is empty. Therefore, $u^n_{i,K} \leq u^\star_{i,K}$ for all $i \in \{1,\dots,I\}$ and all $K \in \mathcal{T}$. □

Theorem 3.3 (Existence of a solution to the scheme)**.** *There exists at least one solution to the scheme* (43)–(45) *complemented with* (38) *satisfying*

$$\pi_\star \leq u^n_{i,K} \leq u^\star_{i,K}, \qquad \forall i \in \{1,\dots,I\},\ \forall K \in \mathcal{T}.$$

Proof. The proof relies on a topological degree argument [18, 9]. Define the functional

$$\boldsymbol{\mathcal{F}}^n : \begin{cases} \mathbb{R}^{I\times \#\mathcal{T}} \times [0,1] \to \mathbb{R}^{I\times\#\mathcal{T}} \\ (\boldsymbol{u},\lambda) \mapsto \left(\mathcal{F}^n_{i,K}(\boldsymbol{u},\lambda)\right)_{i,K} \end{cases} \tag{50}$$

where

$$\begin{aligned} \mathcal{F}^n_{i,K}(\boldsymbol{u},\lambda) =& \lambda\phi_i \frac{\overline{h}_{i,K}(u_{i,K}) - h^{n-1}_{i,K}}{\Delta t_n} m_K \\ & - \lambda(\pi_\star - u_{i,K})^+ + \lambda(u_{i,K} - u^\star_{i,K})^+ + (1-\lambda)(u_{i,K} - \pi_i) \\ & + \lambda \sum_{\sigma = K|L} \tau_\sigma \frac{\kappa_i}{\mu_{\mathrm{o}}} h_{i,\sigma} \left(u_{i,K} - u_{i,L} - \varrho g (b_{i,K} - b_{i,L})\right) \\ & + \lambda \left(\overline{S}_{i,K}(u_{i,K}, u_{i+1,K}) - \overline{S}_{i-1,K}(u_{i-1,K}, u_{i,K})\right) m_K, \end{aligned}$$

where $h_{i,\sigma}$ is defined by (44) but with generic $u_{i,K}$ and $u_{i,L}$ instead of values $u^n_{i,K}$ and $u^n_{i,L}$ of a discrete solution. Because of the Lipschitz continuity of $\overline{h}_{i,K}$ and $\overline{p}_{i,K}$, the functional $\boldsymbol{\mathcal{F}}^n$ is uniformly continuous w.r.t. its two arguments.

Define the relatively compact open set

$$\mathcal{U} = \{\boldsymbol{u} \in \mathbb{R}^{I\times\#\mathcal{T}} \mid \pi_\star - 1 < u_{i,K} < u^\star_{i,K} + 1\}.$$

For $\lambda = 0$, $\boldsymbol{\mathcal{F}}^n(\cdot,0)$ turns out to be linear, and the system $\boldsymbol{\mathcal{F}}^n(\boldsymbol{u},0) = \mathbf{0}$ admits $\boldsymbol{u}^{(0)} = (\pi_i)_{i,K}$ as a unique solution. The topological degree corresponding to $\boldsymbol{\mathcal{F}}^n(\cdot,0)$ and $\mathcal{U}$ is equal to 1 since $\boldsymbol{u}^{(0)}$ belongs to $\mathcal{U}$. Then one can adapt the proof of Lemma 3.2 to show that any solution $\boldsymbol{u}^{(\lambda)}$ to the system $\boldsymbol{\mathcal{F}}^n(\boldsymbol{u}^{(\lambda)},\lambda) = \mathbf{0}$ for $\lambda \in (0,1]$ necessarily belongs to $\mathcal{U}$. Therefore, the topological degree corresponding to $\boldsymbol{\mathcal{F}}^n(\cdot,\lambda)$ and $\mathcal{U}$ does not depend on λ. In particular, it is also equal to 1 for

$\lambda = 1$, ensuring the existence of at least one solution $\boldsymbol{u}^{(1)} = \boldsymbol{u}^n$ to the stabilized scheme (47). Since the stabilization terms vanish on $\mathcal{U}$, $\boldsymbol{u}^n$ is also a solution to the scheme (43). □

3.3.3. *Energy stability of the scheme.* The goal of this section is to establish the following discrete counterpart of Proposition 1.2, namely the decay of the energy if the system is isolated. Here, the discrete energy is noting but the continuous energy $\mathfrak{E}$ defined by (13) applied to the approximate solution $\boldsymbol{h}_\mathcal{D}$ defined by (39).

Proposition 3.4. *Let $\boldsymbol{u}^n$ be a solution to the scheme (43)–(45) complemented with the no-flux boundary conditions (38), then $\mathfrak{E}(\boldsymbol{h}_\mathcal{D}^n) \leq \mathfrak{E}(\boldsymbol{h}_\mathcal{D}^{n-1})$.*

Proof. The proof follows the line of the one of Proposition 1.2. Multiplying the scheme (43) by $\Delta t_n(u_{i,K}^n - \varrho g b_{i,K})$ then summing over $K \in \mathcal{T}$ and $i \in \{1, \dots, I\}$ yields

$$A_\mathcal{T}^n + B_\mathcal{T}^n + C_\mathcal{T}^n = 0,$$

where we have set

$$A_\mathcal{T}^n = \sum_{i=1}^{I} \sum_{K\in\mathcal{T}} m_K \left(h_{i,K}^n - h_{i,K}^{n-1}\right)\left(u_{i,K}^n - \varrho g b_{i,K}\right),$$

$$B_\mathcal{T}^n = \sum_{i=1}^{I} \Delta t_n \sum_{\substack{\sigma\in\mathcal{E}_{\rm int}\\ \sigma=K|L}} \tau_\sigma \frac{h_{i,\sigma}^n}{\mu_{\rm o}} \left|u_{i,K}^n - u_{i,L}^n - \varrho g(b_{i,K} - b_{i,L})\right|^2,$$

$$C_\mathcal{T}^n = \sum_{i=1}^{I-1} \Delta t_n \sum_{K\in\mathcal{T}} m_K S_{i,K}^n \left(u_{i,K}^n - u_{i+1,K}^n - \varrho g(b_{i,K} - b_{i+1,K})\right).$$

The term $B_\mathcal{T}^n$ is obviously non-negative since $h_{i,\sigma}^n \geq 0$. For the term $A_{\mathcal{T}^n}$, let us first remark that since $0 \leq h_{i,K}^n \leq H_{i,K}$, one can rewrite

$$\mathfrak{E}(\boldsymbol{h}_\mathcal{D}^n) = \sum_{i=1}^{I} \sum_{K\in\mathcal{T}} m_K E_{i,K}(h_{i,K}^n)$$

where $E_{i,K}$ is the convex functional defined by

$$E_{i,K}(h) = \begin{cases} \pi_i h + \frac{1}{2}\varrho g \left(b_{i,K} - h\right)^2 & \text{if } 0 \leq h \leq H_{i,K}, \\ +\infty & \text{otherwise.} \end{cases}$$

Given $h \in [0, H_{i,K}]$, the subdifferential of $E_{i,K}$ at h is given by

$$\partial E_{i,K}(h) = \left\{p + \varrho g \left(h - b_{i,K}\right) \mid p \in \widetilde{\pi}_{i,K}(h)\right\}.$$

Therefore, a simple convexity inequality provides

$$A_\mathcal{T}^n \geq \mathfrak{E}(\boldsymbol{h}_\mathcal{D}^n) - \mathfrak{E}(\boldsymbol{h}_\mathcal{D}^{n-1}).$$

As in the continuous case, we decompose

$$C_\mathcal{T}^n = \sum_{i=1}^{I-1} \Delta t_n \sum_{K\in\mathcal{T}} m_K \frac{\kappa_i}{\mu_w \frac{\kappa_i}{\kappa_{i+1}} H_{i+1,K} + \mu_o h_{i,K}^n} \Big(\left(u_{i,K}^n - p_{i+1,K}^n\right)^+ \Big)^2 + \sum_{i=1}^{I-1} \Delta t_n \sum_{K\in\mathcal{T}} m_K S_{i,K}^n (H_{i+1,K} - h_{i+1,K}^n).$$

Both contributions are non-negative, hence so does $C_\mathcal{T}^n$. □

Remark 3.5 (steady states)**.** *It is worth noticing in the proof of Proposition 3.4 that the term $B_{\mathcal{T}}^n$ vanishes iff all the horizontal fluxes vanish, while the term $C_{\mathcal{T}}^n$ vanishes iff all the interlayer vertical fluxes vanish. Therefore, either $\boldsymbol{h}^n$ is steady, i.e., $\boldsymbol{h}^n = \boldsymbol{h}^{n-1}$, or the energy is strictly decreasing. The steady states thus correspond to the solutions whose horizontal and vertical fluxes are both identically equal to 0.*

4. Numerical results

Before presenting numerical outcomes in Sections 4.2 and 4.3, we provide some details in Section 4.1 on the effective resolution of the nonlinear system (43)–(46).

4.1. About the practical resolution.

The nonlinear system (43)–(46) can be rewritten in the compact form $\boldsymbol{\mathcal{G}}^n(\boldsymbol{u}^n) = \mathbf{0}$ with $\boldsymbol{\mathcal{G}}^n = \boldsymbol{\mathcal{F}}^n(\cdot, 1)$, where $\boldsymbol{\mathcal{F}}^n$ is defined by (50). The Jacobian matrix $\mathbb{J}(\boldsymbol{u})$ of $\boldsymbol{\mathcal{G}}^n$ at $\boldsymbol{u} \in \mathbb{R}^{I\times\#\mathcal{T}}$ might be non-invertible as a consequence of the lack of uniqueness highlighted in Section 3.3.1. This prohibits the direct use of Newton's method. Instead, our approach relies on a quasi-Newton method with a regularised approximate Jacobian matrix $\mathbb{J}_\epsilon(\boldsymbol{u})$ defined by $\mathbb{J}_\epsilon(\boldsymbol{u}) = \mathbb{J}(\boldsymbol{u}) + \epsilon\mathbb{I}$ which is invertible. Practically, we choose $\epsilon = 10^{-4}$ in our simulations. Moreover, we know from Theorem 3.3 that there exists a solution $\boldsymbol{u}^n \geq \pi_\star\mathbf{1}$ to the scheme $\boldsymbol{\mathcal{G}}^n(\boldsymbol{u}^n) = \mathbf{0}$. This suggests the following quasi-Newton/projection algorithm.

Given $\boldsymbol{u}^{n-1} \in \mathbb{R}^{I\times\#\mathcal{T}}$, we initialize the sequence $\left(\boldsymbol{u}^{n,k}\right)_{k\geq 0}$ by setting $\boldsymbol{u}^{n,0} = \boldsymbol{u}^{n-1}$. Assume that $\boldsymbol{u}^{n,k}$, then $\boldsymbol{u}^{n,k+1}$ is computed as follows.

Semi-smooth quasi-Newton step. We first compute the intermediate state $\boldsymbol{u}^{n,k+1/2}$ thanks to a quasi-Newton iteration:

$$\boldsymbol{u}^{n,k+1/2} = \boldsymbol{u}^{n,k} + \boldsymbol{w}^{n,k}, \tag{51a}$$

where $\boldsymbol{w}^{n,k}$ solves

$$\mathbb{J}_\epsilon(\boldsymbol{u}^{n,k})\boldsymbol{w}^{n,k} + \boldsymbol{\mathcal{G}}^n(\boldsymbol{u}^{n,k}) = \mathbf{0}. \tag{51b}$$

Since $\boldsymbol{\mathcal{G}}$ is not smooth but merely piecewise smooth, we enforce Newton's iterations to stop at discontinuities of $\mathbb{J}_\epsilon$. For instance, if $u_{i,K}^{n,k} < \pi_i$ and $u_{i,K}^{n,k} + w_{i,K}^{n,k} > \pi_i$, then we set $u_{i,K}^{n+1/2,k} = \pi_i + \bar{\epsilon}$. The parameter $\bar{\epsilon}$ is very small (it is practically set to $\bar{\epsilon} = 10^{-10}$) and is there to give a proper sense to $\mathbb{J}_\epsilon(\boldsymbol{u}^{n+1/2})$.

Projection step. The intermediate state $\boldsymbol{u}^{n,k+1/2}$ is then projected on $\{\boldsymbol{u} \geq \pi_\star\mathbf{1}\}$ by

$$u_{i,K}^{n,k+1} = \max\left(\pi_\star, u_{i,K}^{n,k+1/2}\right), \qquad k \geq 0,\ 1 \leq i \leq I,\ K \in \mathcal{T}. \tag{52}$$

Stopping criterion and adaptive time stepping. As suggested by [2], our stopping criterion is based on the ℓ^1 norm of the residual, namely $\|\boldsymbol{\mathcal{G}}^n(\boldsymbol{u}^{n,k})\|_{\ell^1} \leq 10^{-8}$. In order to increase the robustness of the resolution, we use a classical adaptive time stepping algorithm. If the loop over k has not yet converged after $k_{\max}$ iterations, we reinitialize the procedure but with a modified system corresponding to a reduced time step divided by two w.r.t. the previous attempt. But is the look over k converges with less that $k_{\max}$ iterations, then the time step for the time iteration $n+1$ is chosen as $\Delta t_{n+1} = 2 \times \Delta t_n$. Because of the degeneracy of the problem, the convergence can be rather slow. Therefore, we have to accept a possibly rather

large number of iteration for each time step. This led us to fix $k_{\max} = 40$ in our simulations.

4.2. **A one-dimensional test case.** We propose a one-dimensional test case the goal of which is to highlight the importance of keeping track of the time variable. The geological basin is composed of a superposition of three vertical layers. More precisely the geological Ω_i is given by

$$\Omega_i = \bigcup_{\boldsymbol{x}\in(0,L)} \{\boldsymbol{x}\} \times (b_{i-1}(\boldsymbol{x}), b_i(\boldsymbol{x}))$$

where the functions b_i, $0 \leq i \leq 3$, are given by

$$\begin{aligned} b_0(\boldsymbol{x}) =& 0, \\ b_1(\boldsymbol{x}) =& \frac{H}{6} + \frac{H}{3L}\left(\boldsymbol{x} + \frac{2L}{3\pi}\sin\left(\frac{3\pi}{L}\boldsymbol{x}\right)\right), \\ b_2(\boldsymbol{x}) =& \frac{5H}{6} - \frac{2H}{3L^2}\left(\boldsymbol{x} - \frac{L}{2}\right)^2, \\ b_3(\boldsymbol{x}) =& H. \end{aligned}$$

The distance are given in meters and $L = 10^4\ m$. The geological properties of these vertical layers are given in Figure 4.2. The viscosity of each phases are given in centipoise (cPo) where $1\,cPo$ corresponds to $10^{-3} Pa \cdot s$. The viscosity of the oil phase set to $\mu_o = 11.78\,cPo$ while the viscosity of the water phase is set to $\mu_w = 0.548\,cPo$. The permeability is given is darcy where 1 mdarcy corrrespond to $10^{-12}\ m^2$. The pressure is given in bar where 1 bar correspond to $10^5\ Pa$. The coefficient ρg is given in $bar \cdot m^{-1}$ and is set to $\rho g = 0.01962\ bar \cdot m^{-1}$. The final time of the simulation is set to $10^{12} s$, which corresponds approximately to 31689 years.

Layer	Rock type	ϕ_i	κ_i (mdarcy)	π_i (bar)
Ω_3	Shale	0.2	2	50
Ω_2	Limestone	0.3	10	20
Ω_1	Sandstone	0.25	100	12

TABLE 1. Properties of the geological layer

There is no oil initially in the domain, namely

$$h_i(0, \boldsymbol{x}) = 0, \qquad 1 \leq i \leq 2,\ \boldsymbol{x} \in (0, L). \tag{53}$$

We assume no-flux boundary conditions on the lateral boundary as well as across the top layer, i.e., $S_2(t, \boldsymbol{x}) = 0$. Oil is injected at the bottom of the domain,

$$S_0(t, \boldsymbol{x}) = s_0 1_{0<t<t_0}(t) 1_{L_1 \leq \boldsymbol{x} \leq L_2}(\boldsymbol{x}) \qquad t \geq 0,\ \boldsymbol{x} \in (0, L), \tag{54}$$

where the source is localized between $L_1 = 2500\,m$ and $L_2 = 2600\,m$. We investigate the long time behavior of the model for two different injection regimes:

- a fast injection regime where $s_0 = 0.04\,m.s^{-1}$ and $t_0 = 10^6 s \simeq 11,57$ days.
- a slow injection regime where $s_0 = 2.10^{-7} m.s^{-1}$ and $t_0 = 2.10^{11} s \simeq 6338$ years.

Note that the total quantity of oil at the final time in the domain is the same for both regimes since $\int_0^T S_0(t,\boldsymbol{x})\mathrm{d}t$ takes the same values in both cases. Therefore, reduced models where the time evolution is neglected would compute the same equilibrium for both scenarios. We assume that

$$S_3(t,\boldsymbol{x}) = 0, \qquad t \geq 0,\ \boldsymbol{x} \in (0,L). \tag{55}$$

For the space discretization we consider a uniform discretization with 1200 cells. This source term is discretized by

$$S^n_{0,K} = \frac{1}{m_K \Delta t_n} \int_{t^{n-1}}^{t^n} \int_K S_0(t,\boldsymbol{x})\,\mathrm{d}\boldsymbol{x}\mathrm{d}t, \qquad K \in \mathcal{T}, \tag{56}$$

The evolution of the interfaces between oil and water are represented on Figure 4 and Figure 5 for the fast and slow injection regims respectively. Notice that the final steady state is different in both situations, as predicted in [23].

4.3. **A two-dimensional test case.** We propose a two-dimensional test case where the geological basin is composed of a superposition of two layers. More precisely the geometry of the geological layers Ω_1, Ω_2 is given by

$$\Omega_i = \bigcup_{\boldsymbol{x}\in\mathcal{O}} \{\boldsymbol{x}\} \times (b_{i-1}(\boldsymbol{x}), b_i(\boldsymbol{x})), \quad i \in \{1,2\},$$

where $\mathcal{O} = (0,L)^2$ with $L = 10^4 m$. The interfaces $(b_i)_{0\leq i\leq 2}$ are given by $b_0(\boldsymbol{x}) = 0$,

$$\begin{aligned} b_1(x,y) =& 400\left[\cos\left(\frac{5x}{2L}\right)\sin\left(\frac{2y}{L}\right) + \frac{5}{3}\right], \\ b_2(x,y) =& 400\left[\sin\left(\frac{2x}{L}\right)\cos\left(\frac{5y}{2L}\right) + \frac{10}{3}\right]. \end{aligned}$$

The physical properties of the two different rocks are described in Table 4.3. The physical properties of the two fluids are chosen as in Section 4.2.

Layer	Rock type	ϕ_i	κ_i (mdarcy)	π_i (bar)
Ω_2	Limestone	0.3	10	20
Ω_1	Sandstone	0.25	100	12

TABLE 2. Properties of the geological layer

In each geological layer the height of the oil phase is initially to zero, i.e.,

$$h_i(0,\boldsymbol{x}) = 0, \qquad 1 \leq i \leq 2,\ \boldsymbol{x} \in \mathcal{O},$$

We assume no-flux boundary conditions across the lateral boundaries as well as across the roof, i.e., $S_2 \equiv 0$. Concerning the source term, we consider again a fast and a slow injection regim. For the fast injection regim, oil is injected through a part $\omega = (600, 2400)^2$ of the bottom of the domain at the rate of $12.10^{-6} m \cdot s^{-1}$ between $t = 0$ and $t = 10^8 s \simeq 3,17$ years, leading to the following formula:

$$S_0(t,\boldsymbol{x}) = 12.10^{-6} \times 1_\omega(\boldsymbol{x}) \times 1_{(0,10^8)}(t), \qquad \forall (t,\boldsymbol{x}) \in \mathbb{R}_+ \times \mathcal{O}.$$

The injection zone ω is highlighted in blue on Figure 6.

The set $\mathcal{O}$ is discretized thanks to a 51×51 uniform cartesian grid. We use an adaptive time stepping strategy with time steps between $10^8 s$ and $5.10^{10} s$.

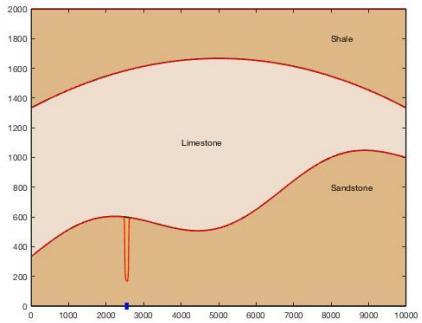

$t = 10800\,s = 3$ hours

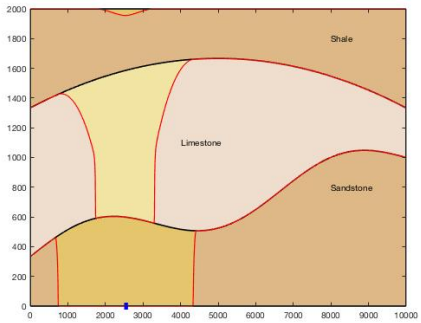

$t = 10^6 s \simeq 11.6$ days

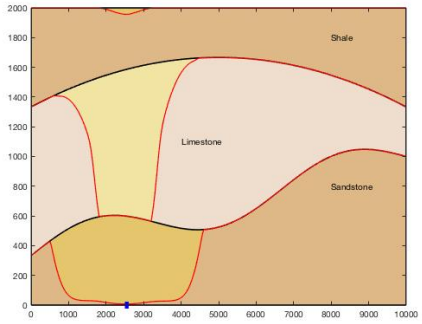

$t = 5.10^6 s \simeq 57.9$ days

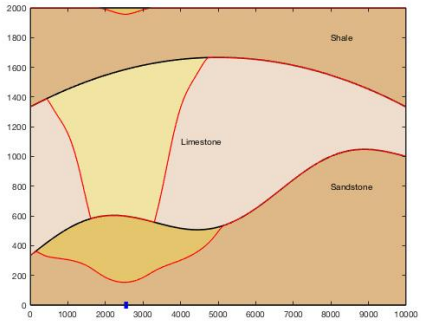

$t = 5.10^7 s \simeq 579$ days

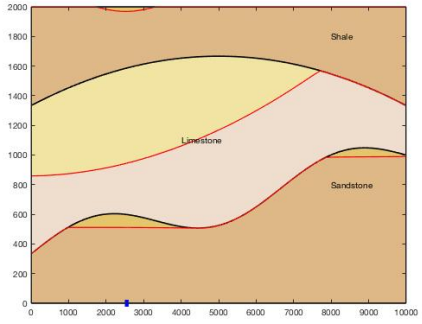

$t = 5.10^9 s \simeq 158.4$ years

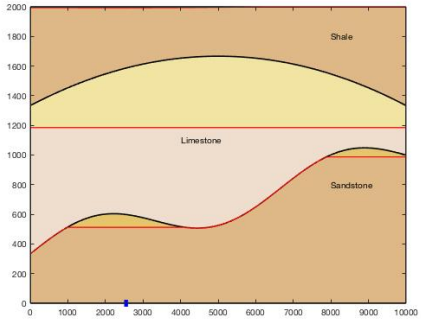

$t = 10^{12} s \simeq 31689$ years

FIGURE 4. Time evolution in the fast injection regim.

The evolution along time of the heights of the interfaces is represented on Figure 6. We notice that It shows that oil invades the upper layer right above the source. This result should be compared to a slow injection regim where

$$S_0(t, \boldsymbol{x}) = 12.10^{-10} \times 1_\omega(\boldsymbol{x}) \times 1_{(0,10^{12})}(t), \qquad \forall (t, \boldsymbol{x}) \in \mathbb{R}_+ \times \mathcal{O},$$

for which the steady state is presented in Figure 7. For this slow injection regim, oil has enough time to creep into the dome located near $(x, y) = (0, 8000)$ and to accumulate there. The total quantity of injected oil (which is the same in both

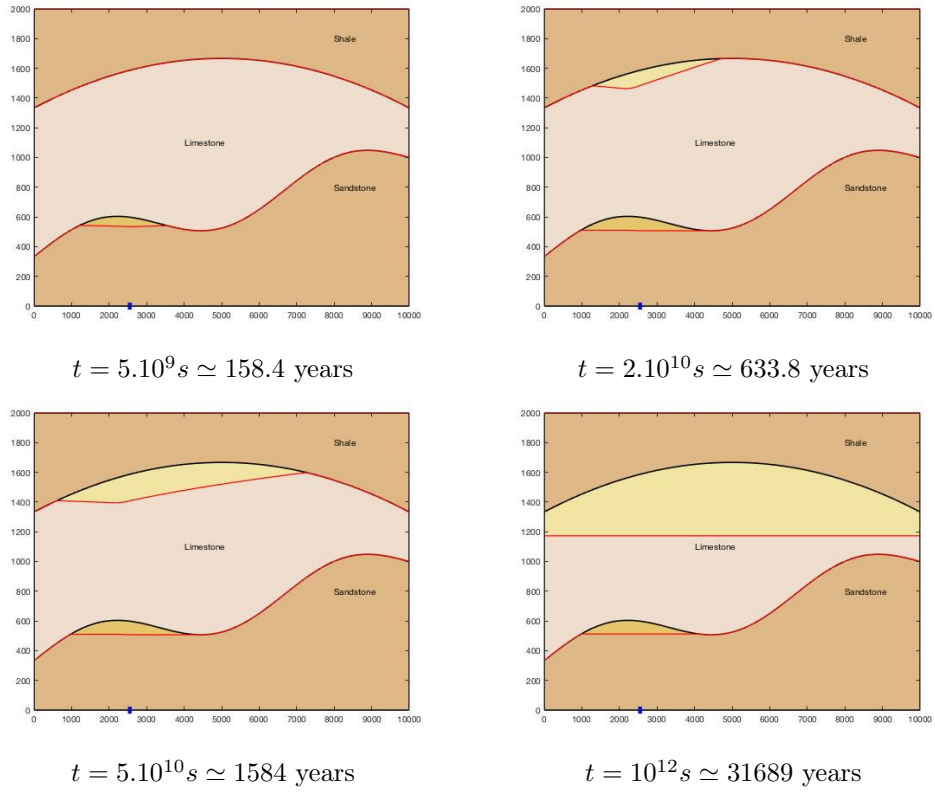

$t = 5.10^9 s \simeq 158.4$ years $\quad$ $t = 2.10^{10} s \simeq 633.8$ years

$t = 5.10^{10} s \simeq 1584$ years $\quad$ $t = 10^{12} s \simeq 31689$ years

FIGURE 5. Time evolution in the slow injection regim.

regims) is not sufficient to reach the critical height $\frac{\pi_2 - \pi_1}{\rho g} \simeq 407.75m$ and the whole oil phase remains therefore trapped in the lower layer.

5. Conclusion

We derived a reduced model accounting time for oil migration in geological basins. Our derivation relies on Dupuit approximation and from a one-dimensional study for the vertical fluxes across the different layers. We proposed an energy stable finite volume scheme for its resolution that required the introduction of an auxiliary variable $\boldsymbol{u}$ for its efficient practical resolution. The numerical results shows that our reduced model is able to reproduce oil trapping generated by capillary pressure discontinuities. They also highlight the importance of taking the time evolution into account. The comparison of our reduced model with full Darcean models should now be performed in order to validate our approach.

Acknowledgements. This work was partially supported by the Labex CEMPI (ANR-11-LABX-0007-01). The authors warmly thank Konstantin Brenner, Guillaume Enchéry and Roland Masson for the shared valuable discussions on the model.

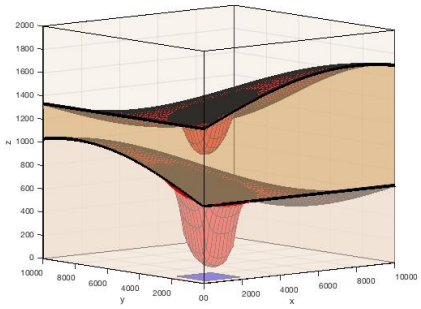

$t = 10^8 s \simeq 3.17$ years

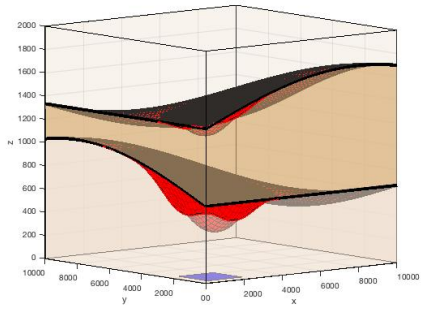

$t = 10^9 s \simeq 31.69$ years

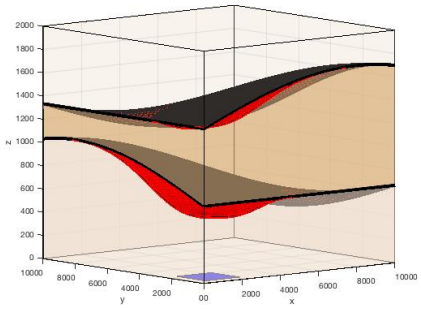

$t = 5.10^9 s \simeq 158.44$ years

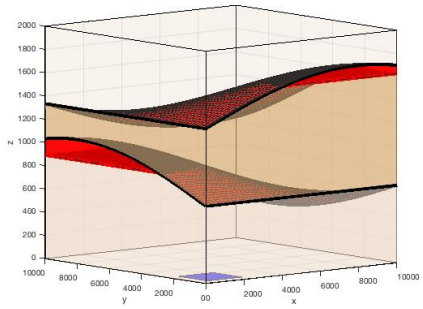

$t = 10^{12} s \simeq 31689$ years

FIGURE 6. Evolution of the model in the two-dimensional setting for the fast injection regim.

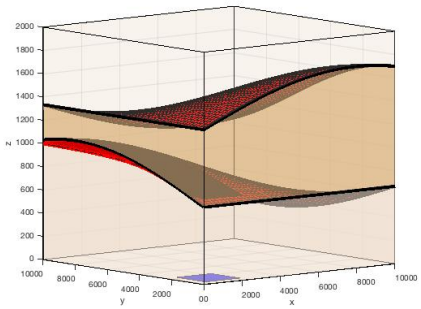

$t = 5.10^{11} s \simeq 15844$ years

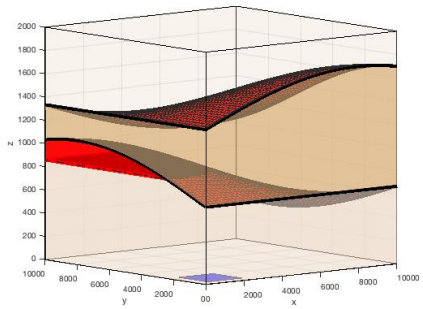

$t = 2.10^{12} s \simeq 63378$ years

FIGURE 7. Evolution of the model in the two-dimensional setting for the slow injection regim.

REFERENCES

[1] J. Bear and Y. Bachmat. *Introduction to modeling of transport phenomena in porous media.* Kluwer Academic Publishers, Dordrecht, The Netherlands, 1990.

[2] K. Brenner and C. Cancès. Improving Newton's method performance by parametrization: The case of the Richards equation. *SIAM J. Numer. Anal.*, 55(4):1760–1785, 2017.

[3] K. Brenner, M. Groza, L. Jeannin, R. Masson, and J. Pellerin. Immiscible two-phase darcy flow model accounting for vanishing and discontinuous capillary pressures: application to the flow in fractured porous media. *Comput. Geosci.*, 21(5-6):1075–1094, 2017.
[4] F. Buzzi, M. Lenzinger, and B. Schweizer. Interface conditions for degenerate two-phase flow equations in one space dimension. *Analysis*, 29:299–316, 2009.
[5] C. Cancès, T. Gallouët, and A. Porretta. Two-phase flows involving capillary barriers in heterogeneous porous media. *Interfaces Free Bound.*, 11(2):239–258, 2009.
[6] C. Cancès, T. O. Gallouët, and L. Monsaingeon. The gradient flow structure of immiscible incompressible two-phase flows in porous media. *C. R. Acad. Sci. Paris Sér. I Math.*, 353:985–989, 2015.
[7] C. Cancès, T. O. Gallouët, and L. Monsaingeon. Incompressible immiscible multiphase flows in porous media: a variational approach. *Anal. PDE*, 10(8):1845–1876, 2017.
[8] C. Cancès and M. Pierre. An existence result for multidimensional immiscible two-phase flows with discontinuous capillary pressure field. *SIAM J. Math. Anal.*, 44(2):966–992, 2012.
[9] K. Deimling. *Nonlinear functional analysis*. Springer-Verlag, Berlin, 1985.
[10] H.-J. G. Diersch and P. Perrochet. On the primary variable switching technique for simulating unsaturated–saturated flows. *Adv. Water Resour.*, 23(3):271–301, 1999.
[11] R. Eymard, T. Gallouët, C. Guichard, R. Herbin, and R. Masson. TP or not TP, that is the question. *Comput. Geosci.*, 18:285–296, 2014.
[12] R. Eymard, T. Gallouët, and R. Herbin. Finite volume methods. Ciarlet, P. G. (ed.) et al., in Handbook of numerical analysis. North-Holland, Amsterdam, pp. 713–1020, 2000.
[13] M. J. Golding, J. A. Neufeld, M. A. Hesse, and Huppert. Two-phase gravity currents in porous media. *J. Fluid Mech.*, 678:248–270, 2011.
[14] M. A. Hesse, F. M. Jr Orr, and H. A. Tchelepi. Gravity currents with residual trapping. *J. Fluid Mech.*, 611:35–60, 2008.
[15] H. E. Huppert and A. W. Woods. Gravity-driven flows in porous layers. *J. Fluid Mech.*, 292:55–69, 1995.
[16] M. Jazar and R. Monneau. Derivation of seawater intrusion models by formal asymptotics. *SIAM J. Appl. Math.*, 74(4):1152–1173, 2014.
[17] R. Juanes, C. W. MacMinn, and M. L. Szulczewski. The footprint of the CO_2 plume during carbon dioxide storage in saline aquifers: Storage efficiency for capillary trapping at the basin scale. *Transp. Porous Med.*, 82:19–30, 2010.
[18] J. Leray and J. Schauder. Topologie et équations fonctionnelles. *Ann. Sci. École Norm. Sup. (3)*, 51:45–78, 1934.
[19] R. J. McCann. A Convexity Principle for Interacting Gases *Adv. Math.*, 128(1):153–179, 1997.
[20] Y. Masson and S. R. Pride. A fast algorithm for invasion percolation. *Transp. Porous Med.*, 102:301–312, 2014.
[21] T. D. Ngo, E. Mouche, and P. Audigane. Buoyant flow of CO_2 through and around a semi-permeable layer of finite extent. *J. Fluid Mech.*, 809:553–584, 2016.
[22] J. M. Nordbotten and M. Celia. *Geological Storage of CO2: Modeling Approaches for Large-scale Simulation*. John Wiley & Sons, New Jersey, 2012.
[23] S. Pegaz-Fiornet. *Study of hydrocarbon migration models for basin simulators*. Theses, Université d'Aix-Marseille, July 2011.
[24] B. Schweizer. Homogenization of degenerate two-phase flow equations with oil trapping. *SIAM J. Math. Anal.*, 39(6):1740–1763, 2008.
[25] Ø. Sylta. New techniques and their application in the analysis of secondary migration. In *Basin Modelling: Advances and Applications*, volume 3, pages 385–398. Elsevier, Amsterdam, 1993.
[26] D. Wilkinson. Percolation model of immiscible displacement in the presence of buoyancy forces. *Phys. Rev. A*, 30(1):520–531, 1984.
[27] D. Wilkinson and J. F. Willemsen. Invasion percolation: a new form of percolation theory. *J. Phys. A: Math. Gen.*, 16:3365–3376, 1983.

Clément Cancès (clement.cances@inria.fr), Inria, Univ. Lille, CNRS, UMR 8524 - Laboratoire Paul Painlevé, F-59000 Lille.

David Maltese (david.maltese@ipsa.fr), Institut Polytechnique des Sciences Avancées, 63 Boulevard de Brandebourg, 94200 Ivry-sur-Seine, France.